Assessing soil erosion of forest and cropland sites in wet tropical Africa using [239+240]Pu fallout radionuclides

Florian Wilken[1,2], Peter Fiener[2], Michael Ketterer[3], Katrin Meusburger[4], Daniel Iragi Muhindo[5], Kristof van Oost[6], Sebastian Doetterl[1]

[1]Department of Environmental Systems Science, Eidgenössische Technische Hochschule Zürich, Zürich, Switzerland
[2]Institute for Geography, Universität Augsburg, Augsburg, Germany
[3]Chemistry and Biochemistry, Northern Arizona University, Flagstaff, USA
[4]Swiss Federal Institute for Forest, Snow and Landscape Research, Birmensdorf, Switzerland
[5]Faculty of Agronomy, Université Catholique de Bukavu, Bukavu, DR Congo
[6]Earth and Life Institute, Université Catholique de Louvain, Louvain-la-Neuve, Belgium

Correspondence to: Florian Wilken (florian.wilken@usys.ethz.ch)

Abstract

Due to the rapidly growing population in tropical Africa, a substantial rise in food demand is predicted in upcoming decades, which will result in higher pressure on soil resources. However, there is limited knowledge on soil redistribution dynamics following land conversion to arable land in tropical Africa that is partly caused by challenging local conditions for long-term landscape scale monitoring. In this study, fallout radionuclides [239+240]Pu are used to assess soil redistribution along topographic gradients at two cropland sites and at three nearby pristine forest sites located in the DR Congo, Uganda and Rwanda. In the study area, a relatively high [239+240]Pu baseline inventory is found (mean forest inventory 41 Bq m^{-2}). Pristine forests show no indication for soil redistribution based on [239+240]Pu along topographical gradients. In contrast, soil erosion and sedimentation on cropland reached up to 37 and 40 cm within the last 55 years, respectively. Cropland sites show high intra-slope variability with locations showing severe soil erosion located in direct proximity to sedimentation sites. This study shows the applicability of a valuable method to assess tropical soil redistribution and provides insight on soil degradation rates and patterns in one of the most vulnerable regions of the World.

1. Introduction

Soil erosion is considered to be the major threat to global soil resources and substantially contributes to crop yield reduction (Amundson et al., 2015; Montanarella et al., 2016; Govers et al., 2017), which challenges food security in regions facing population growth beyond sustainable limits in the 21st century. In particular, the White Nile-Congo rift (NiCo) region faces a strong impact of soil erosion (Lewis and Nyamulinda, 1996; FAO and ITPS, 2015; Montanarella et al., 2016) due to steep terrain, high rainfall erosivity and low soil cover conditions throughout the cultivation period (Lewis and Nyamulinda, 1996). The region is also predicted to undergo substantial climate change, which might further increase soil erosion (Borrelli et al., 2020). The loss of soil resources and yield decline in the NiCo region goes hand in hand with a rapid population growth (population of Rwanda, Uganda and Democratic Republic of Congo 2020: 150 millions – predicted 2100: 430 millions; WPR, 2020), which drives rising food demands that are expected to triple for entire Sub-Saharan Africa between 2010 and 2050 (van Ittersum et al., 2016). The associated pressure on land resources leads to various problems that will have a dramatic ecological and social impact (food insecurity, political unrest, migration) in the NiCo region (Chamberlin et al., 2014; FAO and ITPS, 2015). Under current practices, an increasing demand in food is typically compensated through deforestation to assess new non-degraded soils, which are often located in areas with steep slopes (Govers et al., 2017). This causes a loss of highly valuable forest ecosystem services (e.g. carbon storage, biodiversity, imbalance of the hydrological cycle) and the onset of soil erosion (Nyssen et al., 2004). In steep cropland sites of the NiCo region, it is frequently observed that the entire deep tropical saprolite body is removed and the bedrock is exposed at the surface, which means a quasi-permanent loss of cropland and potential reforestation areas on decadal to centennial timescales (Evans et al., 2020). A pressing need persists to predict future dynamics and timescales of cropland degradation in order to understand the pace of a rising food shortage and to develop adapted agricultural management strategies. Smart intensification of existing cropland soils due to adapted agricultural practices in suitable locations and the conservation/restoration of soils prone to erosion (e.g. reforestation or grassland use) has been discussed as a key management strategy to combat degradation (Govers et al., 2017). A cornerstone to develop a smart intensification plan is detailed information on soil degradation dynamics of specific regions under specific conditions (e.g. land use, topography, soil type, rainfall characteristics). Soil erosion plot experiments were carried out in tropical Africa (Lewis and Nyamulinda, 1996; Xiong et al., 2019) to understand the rates of soil loss. However, plot experiments are limited to soil erosion processes, while soil redistribution dynamics (interaction of erosion and sedimentation) remain unexplained, but are important to understand soil degradation rates on a landscape-scale. However, catchment monitoring that provides insight of internal soil redistribution dynamics necessitates a sufficiently long time series (years to decades) to integrate a statistically representative variety of erosive rainfall events impacting different land cover conditions (Fiener et al., 2019). Particularly in regions of limited infrastructure, long-term catchment monitoring projects are challenging and typically rare. This problem can be overcome by fallout radionuclides from nuclear weapon tests (i.e. ^{137}Cs, $^{239+240}$Pu) as soil redistribution tracers (Meusburger et al., 2016; Alewell et al., 2017; Evrard et al., 2020), which have the major advantage to provide insight on spatial patterns of both soil erosion and sedimentation processes integrated over the period since 1963-1964 (Test Ban

Treaty that caused a rapid decrease of atmospheric bomb tests; Wallbrink and Murray, 1993; Evrard et al., 2020). The most widely used fallout radioisotope in soil redistribution studies is ^{137}Cs (e.g. Porto and Walling, 2012; Chartin et al., 2013; Evrard et al., 2020), which has a rather short half-life of about 30 yrs. Hence, decay has already led to a pronounced reduction (73% in 2020) of the activity until today (Alewell et al., 2017). In tropical regions, this is a critical limitation of using ^{137}Cs for soil

65   redistribution analysis due to a much lower fallout compared to the mid latitudes of the northern hemisphere (Hardy et al., 1973; Evrard et al., 2020). Furthermore, extreme soil erosion rates in the tropics (Lewis and Nyamulinda, 1996; Angima et al., 2003; Nyesheja et al., 2019; Xiong et al., 2019) additionally depleted ^{137}Cs inventories. Over the past decade, the fallout radionuclides ^{239}Pu and ^{240}Pu have been discussed and tested as an alternative radioisotopic tracer to ^{137}Cs for soil redistribution studies. The major advantage of both isotopes is the long half-life (^{239}Pu = 24110 yrs, ^{240}Pu = 6561 yrs) without relevant decay.

70   Furthermore, ^{239}Pu and ^{240}Pu show a very limited plant uptake (Akleyev et al., 2000) and preferentially form associations with soil iron oxides (Ryan et al., 1998; Lal et al., 2013), which potentially makes the isotopes very suitable tracers for tropical environments dominated by Ferralsols. Hence, the $^{239+240}$Pu activity in tropical soils might be high enough to successfully carry out soil redistribution studies and provide an important insight on soil redistribution dynamics in tropical Africa. Few fallout radionuclide based soil redistribution studies have been carried out in the Tropics (Evrard et al., 2020) where, to our best

75   knowledge, non was located in the wet Tropics of Africa (Af, Am climate; Kottek et al., 2006).

In our study we follow two major aims: (i) Testing the suitability of ^{239}Pu and ^{240}Pu as a soil redistribution tracers in the wet Tropics of Africa, and (ii) exemplarily analysing the soil redistribution dynamics following conversion from forest to cropland in the East African NiCo region.

2. Methods

80   ### 2.1 Study sites and sampling design

The NiCo region is located in the headwater catchments of the White Nile (Lake Eduard) and the Congo River (Lake Kivu) that are part of the East African Rift Valley system (Fig. 1). The region faces rapid population growth creating substantial pressure on land resources and initiating forest to cropland conversion. Soil degradation by water erosion is a recognised problem in the region (Lewis and Nyamulinda, 1996; Montanarella et al., 2016) indicated via frequent soil erosion events

85   resulting in ephemeral rills and gullys as well as permanent deep gully systems. The region is characterised by steep terrain (Fig. 1) and tropical climate with a mean annual air temperature between 16.7 and 19.3°C and an annual rainfall sum ranging between 1400 and 1900 mm. The seasonal rainfall distribution is subdivided in two rain and two corresponding dry seasons (Fick and Hijmans, 2017). The rainfall erosivity in the region is high due to frequently occurring storm events of large rainfall amounts linked to high rainfall intensities during the rain seasons (on average 20 erosive rainfall events per rain season; events

90   exceeding 10 mm h^{-1} of rainfall per 30 min interval). Soils in the region are deeply weathered Ferralsols (> 6 m; WRB, 2006; Doetterl et al., 2021) developed from three geochemically distinct parent materials (DR Congo: mafic magmatic rocks; Uganda: felsic magmatic rocks; Rwanda: sedimentary rock of mixed geochemical composition). Soils throughout the study

area are typically classified as clay loam while at the Ugandan forest and cropland study sites a lower clay and higher sand content is found (Doetterl et al., 2021).

95   The forest sites in the study area are primary tropical mountain forests (for detailed information see Doetterl et al., 2021). Farming is documented since the 1950th for the site in DR Congo, while conversion to cropland at the Ugandan site took place during the 1970th (personal communication with local villagers). The cropland sites represent the typical smallholder farming found in the region, which is based on small fields with non-mechanised tillage practices. Due to the small fields (mean field size = 450 m^2) and an individual and dynamic field management, soil cover conditions are very patchy and can alternate

100 between bare soil and fully grown vegetation cover in direct proximity (Fig. 1).

In 2018, a soil sampling campaign was carried out in three pristine forests and two cropland sites in the NiCo region in order to collect soil samples for a soil redistribution assessment based on the fallout radionuclides ^{239}Pu and ^{240}Pu. As part of this campaign, a total of 347 samples were taken. Soil sampling was carried out using a manual closed tube soil corer (VSI soil

105 core sampler, Vienna-Scientific, Austria) with a diameter of 6.8 cm and a length of 120 cm.

Sampling sites in forests were located within the Kahuzi Biega (DR Congo), Kibale (Uganda) and Nyungwe Forest (Rwanda) National Parks (Fig. 1). There, the sampling scheme is aligned to a toposequence approach that covers three different landscape positions situated along a catena: the plateau, slope (up to 30°) and foot-slope. Sampling was carried out at 19 locations within each catena and covers different soil layers (L-horizon, O-horizon and mineral soil; see Tab. 1). Discrete sampling at plateau

110 locations took place in order to understand variation of radionuclide inventories at sites. To average out the typical variability of fallout radionuclide inventories, composite samples were taken at the slope and foot-slope positions. In addition to mineral soil layers, two organic layers at two different levels of decomposition (L and O horizon) were collected over an area of 20 cm x 20 cm at each sampling site. About 40% of the total forest samples were taken at plateau positions (high proportion due to non-composite sampling), while 30% of the samples were taken at slope and foot-slope locations, respectively. At foot-slope

115 locations soils were additionally sampled from 60 cm to 120 cm soil depth to cover colluvial sites with $^{239+240}$Pu activity in the subsoil.

Sampling sites in cropland were placed along two catenae within DR Congo and in Uganda, covering 51 individual locations at each study site (Tab. 1). The majority (~50%) of sampling sites are distributed along slope positions (12-13° steepness in both cropland sites) while 25% of sites are located at foot-slope and plateau sites. To understand the depth distribution of

120 $^{239+240}$Pu and the variability of radionuclide inventories under stable geomorphic conditions, three depth increments of 20 cm thickness were taken to a total soil depth of 60 cm at plateau sites. In DR Congo, a cropland site (converted to grassland approximately in 2005) located about 8 km apart from the study slope was sampled, while in Uganda, flat plateau sites under arable use in direct proximity to the study slope were sampled. At slope locations, a single soil increment down to 60 cm was taken. At the foot-slope locations, to cover potential sedimentation, an additional increment from 60 to 100 cm was sampled

125 to assure full cover of the radionuclide inventory.

2.3 $^{239+240}$Pu measurements

An assessment of fallout radionuclides $^{239+240}$Pu inventories was used to estimate effective soil redistribution since the 1960s along the investigated geomorphic transects. Plutonium isotopes measurements were conducted following Calitri et al. (2019) and Ketterer et al. (2004). The chemical preparation consisted of the following sequence:

130 1. Soil material was milled and subsequently dry-ashed for at least eight hours at 600°C to remove organic matter. An aliquot of the dry-ashed material of up to 50 grams was weighed into a 250 mL polypropylene bottle. Samples were tested for excessive reaction of carbonates by addition of 5 mL of 8 M HNO_3.

2. Samples were spiked using 7 picograms (~ 1 mBq) of a ^{242}Pu tracer (NIST 4334g), in the form of a solution in 4 M aqueous HNO_3.

135 3. 125 mL of 8 M aqueous HNO_3 were added, with caution being exercised to add acid slowly when carbonates were present.

4. The sample vessels were capped and heated at 80°C overnight (~ 16 hours) with occasional mixing.

5. Following heating, the sample leach solutions were recovered by filtration with 0.45 micron cellulose nitrate membranes.

6. The plutonium was converted to the +4 oxidation state via addition of 0.5 g $FeSO_4 \cdot 7H_2O$ dissolved in 2 mL water, followed by 2 grams of $NaNO_2$ dissolved in 5 mL water. Thereafter, the solutions were heated uncapped in a 90° C convection oven

140   for 1.5 hours to release evolved NO_2 (g) and allow for conversion of the Pu into Pu(IV).

7. 300 milligrams of Pu-selective resin TEVA (EIChrom, Lisle, IL, USA) was added to the sample solution; the mixtures were agitated over a 4-hour timeframe to allow for the resin to uptake the Pu(IV).

8. The TEVA resin was collected on a 20 mL polyethylene column equipped with a glass wool plug; the pass-through solution was drained and discarded. The columns were rinsed with the following sequence: i) 50 mL of 2 M aqueous HNO_3; ii) 20

145   mL of 9 M aqueous HCl; and iii) 10 mL of 2 M aqueous HNO_3. The rinse sequence removes matrix elements, uranium and thorium.

9. Plutonium was eluted from the columns using the following sequence: i) 0.5 mL water; ii) 0.5 mL of 0.05 M aqueous ammonium oxalate; and iii) 0.5 mL water, all of which were collected together for analysis directly after elution.

In the preparations, quality control samples were included to assess the results; these consisted of blanks (35 g powdered

150 sandstone devoid of detectable Pu). Blanks consisting of 35 g sandstone spiked with small quantities (50-100 milligrams) of IAEA 384 (Fangataufu Sediment) were also prepared. Eleven measurements of IAEA 384 resulted in an average of 102 Bq kg^{-1} $^{239+240}$Pu, and a standard deviation of 10 Bq kg^{-1}; these results compare well to the reference value of 107 Bq kg^{-1} $^{239+240}$Pu. The blanks were used to determine a detection limit of 0.01 Bq kg^{-1} $^{239+240}$Pu.

Sample Pu fractions were measured with a Thermo X Series II quadrupole ICP-MS (Bremen, Germany) equipped with an

155 APEX HF high-efficiency sample introduction system (ESI Scientific, Omaha, NE, USA). The APEX is equipped with a self-aspirating concentric fluorinated ethylene-propylene nebulizer operating at an uptake rate of ~ 0.15 mL per minute. The instrument is located at Northern Arizona University; the laboratory is licensed with the State of Arizona for handling ^{242}Pu spike solutions. The intensities of ^{235}U, ^{239}Pu, ^{240}Pu and ^{242}Pu were recorded using a peak-jump algorithm (10 ms dwell time,

1000 sweeps/integration, three integrations per sample). The ^{235}U isotope was measured as a proxy for ^{238}U, the latter whose
intensity occasionally exceeded the linear range of the ICPMS's pulse-counting detector; this was done in order to assess the
potential interference of ^{238}U^{1}H$^+$ on ^{239}Pu. As many samples exhibited relatively high levels of ^{238}U^{1}H$^+$, generating a potential
"false-positive" detection of ^{239}Pu, it was determined to be advantageous to measure Pu using the ^{240}Pu isotope, which is
unaffected by uranium hydride species. The measured atom ratio ^{240}Pu/^{242}Pu was converted into a mass of ^{240}Pu detected, using
the known mass of ^{242}Pu; the ^{240}Pu activity was calculated, and converted into the corresponding $^{239+240}$Pu activity, based on
the known ^{240}Pu/^{239}Pu atom and activity ratios in stratospheric fallout Pu (Kelley et al., 1999). The method resulted in a
detection limit of 0.01 Bq kg^{-1} $^{239+240}$Pu, which equates to a soil inventory of ca. 5-8 Bq m^{-2} $^{239+240}$Pu for a bulk density of ~0.8
to ~1.3 Mg m^{-3}.

2.4 Cropland soil redistribution calculation

To derive topographic change and corresponding soil redistribution using $^{239+240}$Pu inventories, a mass balance model (Zhang
et al., 2019) was applied integrating soil erosion and sedimentation over the period 1964 to 2018. To account for the different
nature of soil erosion and sedimentation processes, the processes were individually implemented (R-Core-Team, 2019) as
follows below.

Due to topsoil loss by soil erosion, former subsoil with negligible low $^{239+240}$Pu activity gets increasingly incorporated into the
plough layer. This exponential decay of the $^{239+240}$Pu inventory is mainly controlled by the soil erosion magnitude and
frequency and plough depth. These process are addressed by the mass balance model that simulates the $^{239+240}$Pu inventory
reduction on a year by year basis over the simulation period:

$$A_{yr} = \int_{1964}^{yr} A_{yr-1963} \left(1 - \frac{R_{yr}}{d}\right)$$

where yr is the simulation year, A_{yr} is the $^{239+240}$Pu inventory at the specific simulation year in Bq m^{-2}, $A_{yr-1963}$ is the annually
updated $^{239+240}$Pu inventory in Bq m^{-2}, d is the average plough depth in m, R_{yr} is soil erosion of simulation year in m. Based
on these results, an individual logarithmic function between A and R for each study site was fitted that can be used to derive
the amount of soil loss in cm (55 yrs.)$^{-1}$.

Sedimentation is represented as a linear increase of the inventory:

$$R = -d\left(1 - \frac{A}{A_{ref}}\right)$$

where R is the soil redistribution rate in m (55 yrs)$^{-1}$ and A is the $^{239+240}$Pu activity difference (reference vs. local activity) in m
x m (55 yrs)$^{-1}$ and Bq kg^{-1} x Bq kg^{-1} (55 yrs)$^{-1}$ over the simulation period.

Finally, the $^{239+240}$Pu activity (Bq m^{-2}) was converted from topographic change (in m) into soil redistribution rates Y in Mg ha^{-1} (55 yrs)$^{-1}$ as follows (Walling et al., 2011):

$$Y = 10\, d\, B \left(1 - \frac{R}{d}\right)$$

where B is the bulk density in kg m^{-3}. B is measured for each mineral and O-horizon sample, while B for the L layer was taken from literature 80 kg m^{-3} (Wilcke et al., 2002).

2.5 Cropland scenario assessment using a mass balance model

The mass balance soil mixing model was used to assess different scenario assumptions and their sensitivity. First, different $^{239+240}$Pu reference inventories were determined in two ways: (i) the mean $^{239+240}$Pu inventory of all forest sites of a specific region (Ref$_{for}$; i.e. mean inventory of Kahuzi Biega forest for the DR Congo cropland sites and Kibale forest for the Ugandan cropland sites) and (ii) the mean $^{239+240}$Pu inventory of the cropland plateau sites of the specific region (Ref$_{plt}$). Second, the sensitivity of the ploughing and corresponding mixing depth is assessed using a 20±5 cm ploughing depth deviation. Third, to address potential interannual variability of water erosion, a scenario with five extreme years producing the same total soil erosion as a 55 years continuous soil erosion rate was compared against the results of the first scenario.

3. Results

$^{239+240}$Pu activities and inventories of forest sites

The mean inventory (i.e. sum of L, O and mineral horizons $^{239+240}$Pu activities) of all forest sampling sites is 41.3 Bq m^{-2}, whereas the measured $^{239+240}$Pu activity in the Kahuzi Biega forest is somewhat smaller compared to the Kibale and Nyungwe forests (Fig. 3; Kahuzi Biega: 32.7 Bq m^{-2}, Kibale: 42.9 Bq m^{-2}; Nyungwe: 48.4 Bq m^{-2}). The majority of L horizon samples fall below the $^{239+240}$Pu detection limit (0.01 Bq kg^{-1}; 40 out of 55 samples). O horizon samples show distinctively higher $^{239+240}$Pu activities (Fig. 2). However, the contribution of the O horizons to the $^{239+240}$Pu inventory of the soil profile is small (mean: 1.2%), because of low bulk density (approx. 0.2 Mg m^{-3}) and O horizon thickness (mean 5 cm). $^{239+240}$Pu activities of the 0 to 60 cm depth mineral soil layers fall rarely below the detection limit (7 of 55 samples), while the $^{239+240}$Pu activities of samples within the detectable range are at least three times higher than the detection limit (Fig. 3). In contrast, almost no activity is detected in the subsoil layer from 60 to 120 cm.

Comparing the $^{239+240}$Pu activities at different topographic positions does not result in a consistent $^{239+240}$Pu activity to topography relation (Fig. 2). While the foot-slopes in Rwanda show the highest $^{239+240}$Pu activities, the opposite is the case for foot-slopes in Uganda and DR Congo. At the plateau sites in Uganda and Rwanda, a lower $^{239+240}$Pu activity compared to the slope sites is found. The mean inventories found at the slope and foot-slope within each forest fall within the range of one standard deviation ± mean $^{239+240}$Pu activity of the region specific plateau sites (Fig. 2). The only exception is the foot-slope in the Ugandan forest that falls in range by two standard deviations of the plateau mean.

$^{239+240}$Pu activities and inventories of cropland sites

At both cropland study sites, a distinctively lower $^{239+240}$Pu activity relative to the forest sites is found. The lowest activity of
220     $^{239+240}$Pu is found at slope positions in DR Congo where 50% (n = 16) of sampling sites fall below the detection limit. The
measurable slope samples show a mean and standard deviation of 0.019±0.006 Bq kg^{-1}. A pronounced increase of the $^{239+240}$Pu
activities can be observed at foot-slope positions with activity also detectable in the sampled 60-100 cm subsoil layer (Fig. 2).
Hence, the $^{239+240}$Pu activity at the DR Congo cropland site follows a topography related spatial pattern from low activities at
slope to elevated activities at foot-slope positions.

225   In comparison to the cropland study site in DR Congo, the activities at the Ugandan cropland site are much higher (mean
$^{239+240}$Pu activity at slope sites DR Congo: 0.012 Bq kg^{-1}, Uganda: 0.046 Bq kg^{-1}) and do rarely (3 of 44 samples) fall below
the detection limit. Variability of $^{239+240}$Pu activities at Ugandan site is extremely high and shows for slope positions a
coefficient of variation of 76%. In contrast to DR Congo cropland, lower $^{239+240}$Pu activities are found at Ugandan foot-slope
sites compared to slope positions (Fig. 2). Furthermore, the Ugandan foot-slope positions showed almost no $^{239+240}$Pu activity
230   in the subsoil layer of 60-100 cm soil depth (Fig. 2).

DR Congo plateau sites (Ref$_{plt}$), assumed to represent the preserved full inventory of the global fallout, show a substantially
lower $^{239+240}$Pu inventory compared to the about 30 km apart located forest sites (DR Congo Ref$_{plt}$: 8.0 Bq m^{-2} vs. mean forest
Ref$_{for}$: 32.7 Bq m^{-2}). Similar, Uganda cropland plateau sites $^{239+240}$Pu inventory (24.4 Bq m^{-2}) are lower compared to nearby
(~10 km) forest sites, but with a lower relative difference compared to their DR Congo counterparts (relative difference Ref$_{for}$
235   vs. Ref$_{plt}$: Uganda 43%, DR Congo 75%). The $^{239+240}$Pu activity below the 0 - 20 cm topsoil layer at the plateau sites in DR
Congo show a sharp reduction of the $^{239+240}$Pu activity in subsoil (Fig. 2), while at the Ugandan cropland sites, soil layers down
to 40 cm show significant $^{239+240}$Pu activity.

Cropland soil erosion and sedimentation
240   An important piece of information that is provided by the erosion module of the mass balance model is the minimum quantity
of soil loss that is required to cause a reduction of the $^{239+240}$Pu inventory that falls below the detection limit after the model
integration period of 55 yrs. The difference between the Ref$_{for}$ and the Ref$_{plt}$ $^{239+240}$Pu baseline reference leads to substantial
differences in modelled erosion. The model indicates that at the DR Congo cropland sites, soil loss of at least 37 cm (55 yrs.)$^{-1}$ is necessary before the $^{239+240}$Pu activity falls below detection limit using Ref$_{for}$ and in contrast 10 cm (55 yrs)$^{-1}$ using Ref$_{plt}$.
245   At the Ugandan cropland sites, a $^{239+240}$Pu inventory reduction to reduce activity below detection limit is found for 43 cm soil
loss (55 yrs.)$^{-1}$ when applying Ref$_{for}$ and 32 cm (55 yrs)$^{-1}$ when applying Ref$_{plt}$, respectively (Fig. 4).

Also, a pronounced sensitivity of the mass balance model on the tillage depth parameter is found. A deviation from an assumed
20 cm plough depth of ±5 cm causes a change of the required soil loss until the detection limit is reached of about ±24%.
Testing the concentrated scenario (only 5 extreme erosion years within 55 years simulation period), showed that detection
250   limit is reached after 19% less total soil loss. Hence, the sensitivity of the ±5 cm plough depth exceeds the impact of the erosion
year frequency, even for this extreme scenario assumption in the NiCo ecosystem (approx. 20 erosive rainfall events per rain
season).

The number of sampling sites that are considered to be subject to sedimentation is widely controlled by the assumption on the applied reference (Ref_{for} and Ref_{plt}). When using Ref_{for}, 4 sloping sites (DR Congo: 0, Uganda: 4) show sedimentation greater than 5 cm (55 yrs)$^{-1}$. This number increased to 24 sites following Ref_{plt} (DR Congo: 9, Uganda: 15). For both reference scenarios, sedimentation at sloping positions is much weaker in DR Congo as compared to Ugandan cropland (Fig. 5). The foot-slope sites in DR Congo show distinctively higher $^{239+240}$Pu inventories compared to the slope sites (Fig. 5). However, the mean inventory of foot-slope positions is still lower than the Ref_{for} $^{239+240}$Pu inventory (28 vs. 32 Bq m^{-2}), which would be interpreted as an indicator for weak soil erosion considering Ref_{for} for soil redistribution calculation. In contrast, if Ref_{plt} is used in the calculation, the same foot-slope positions would be interpreted as sites that received substantial sedimentation exceeding 40 cm (55 yrs)$^{-1}$ (Fig. 5). The foot-slope sites in DR Congo show a pronounced $^{239+240}$Pu activity in many subsoil samples (60-100 cm), while no such subsoil $^{239+240}$Pu activity is found at foot-slope sites of the Ugandan study site (Fig. 2). Simulated sedimentation that exceeds the site specific sampling depth minus the plough depth (i.e. 40 cm at the slope locations assuming a 20 cm plough depth) is rarely found for both reference assumptions (DR Congo Ref_{plt}: 1, Ref_{for}: 0; Uganda Ref_{plt}: 6, Ref_{for}: 2) and therefore suggests a limited impact of enrichment processes by selective transport.

4. Discussion

Applicability of $^{239+240}$Pu as soil erosion tracer in Tropical Africa

Within this study, a $^{239+240}$Pu based soil redistribution analysis at three forest and two cropland sites in the NiCo region was carried out. It is shown that for the majority of samples the topsoil $^{239+240}$Pu activity is high enough to be successfully measured and provide insight on soil redistribution in Tropical Africa over the past decades. To our knowledge, this is the first $^{239+240}$Pu based soil redistribution study in Tropical Africa.

The $^{239+240}$Pu inventory findings in this study are much higher than expected based on the global fallout estimates reported by Kelley et al. (1999) and Hardy et al. (1973) (4.8 Bq m^{-2} and 11.1 Bq m^{-2} for 10°N and 10°S). For the latitudinal classification of Hardy et al. (1973) only two measurements between 10°N and 10°S were located in Africa (Muguga, Kenya & Luanda, Angola; Hardy et al., 1973; Kelley et al., 1999). Both stations receive a substantially lower annual precipitation (960 and 430 mm for Kenya and Angola, respectively) than the NiCo region (>1400 mm yr^{-1}; Fick and Hijmans, 2017) and show contrasting $^{239+240}$Pu inventories of 19.2 Bq m^{-2} in Kenya and 3.4 Bq m^{-2} in Angola. Hence, it is not surprising to find higher baseline $^{239+240}$Pu inventories within the NiCo region than in Kenya or Angola. The three pristine forests show mean $^{239+240}$Pu inventories between 33 and 48 Bq m^{-2} (DR Congo: 32.7±7.7 Bq m^{-2}; Uganda: 42.91±15.5 Bq m^{-2}; Rwanda: 48.4±18.2 Bq m^{-2}), which is sufficiently high for soil redistribution studies.

However, half of the slope sites (14 of 28) at the cropland site in DR Congo fall below the detection limit (0.01 Bq kg^{-1}; ~5 Bq m^{-2}). This is partly caused by the sampling design of this study, which is based on large and deep single soil increments that cover the soil depth from 0 to 60 cm and 60 to 100 cm at the slope and foot-slope positions. A straightforward way to increase the $^{239+240}$Pu activity in the sample is the reduction of the sample increment depth for a corresponding increase of the topsoil

285   proportion that has a higher $^{239+240}$Pu activity (see 20 cm increments taken at cropland plateau sites Fig. 2). However, a reduction of the sampling increments necessarily requires an additional subsoil analysis in highly degraded soil systems, particularly in regions with complex soil redistribution patterns to cover the full $^{239+240}$Pu inventory.

$^{239+240}$Pu reference inventory

290   Within this study, two different reference scenarios are taken into account: (i) Ref_{for} mean of specific forest sites (ii) and Ref_{plt} mean of cropland plateau positions of the specific sites. A high variability of $^{239+240}$Pu activities and corresponding inventories in three pristine tropical forests within similar topographic positions that exceeds differences in Pu inventories along slope positions is found (Fig. 2). The variation of forest $^{239+240}$Pu inventories due to bioturbation and fallout infiltration patterns (e.g. caused by through fall or stem flow patterns) exceeds a potential soil redistribution impact, which is illustrated by the standard

295   deviation of the plateau sites that covers the variability of the slope and foot-slope composite samples (Fig. 2). Additional evidence that soil redistribution processes in the studied forest systems are small is that no major differences between chemical and physical soil properties are found along geomorphic gradients (Reichenbach et al., 2021). This finding is in line with global erosion plot studies from tropical forest plots (mean erosion 0.2 Mg ha^{-1} yr^{-1}, 39 plots with 116 plot years; Xiong et al., 2019). Observations on sediment delivery monitoring in the NiCo region show that the amount of sediment delivery from pristine

300   forests is typically less than 1 Mg ha^{-1} yr^{-1} (personal communication with Simon Baumgartner, UCL runoff monitoring FORSEDCO project). Furthermore, Drake et al. (2019) exemplarily showed in the NiCo region that particular matter export within pristine tropical forest catchments are dominated by organic matter export with little to no mineral sediment being transported. In contrast, partly deforested catchments with agricultural use show substantial carbon delivery by organo-mineral complexes that indicates detachment and transport of the mineral soil layers, which is again in line with the soil erosion results

305   of this study (Drake et al., 2019). Hence, the forest sites are assumed to represent almost the entire $^{239+240}$Pu inventory of the global fallout. The basic assumption behind the reference sites is that the full inventory is preserved as no soil redistribution has taken place and the $^{239+240}$Pu inventories of both Ref_{for} and Ref_{plt} are supposed to be similar. However, the mean cropland plateau $^{239+240}$Pu inventory in Uganda is about half (24.4±7.6 Bq m^{-2}) and in DR Congo only a quarter (8.0±1.0 Bq m^{-2}) of the mean inventories found in the nearby (<30 km) pristine forest sites (Fig. 3), which cannot be explained by local rainfall and

310   corresponding fallout patterns. Subsoil below 60 cm depth at cropland foot-slope positions show $^{239+240}$Pu activity, which is a clear proxy for substantial sedimentation (Fig. 2). However, the $^{239+240}$Pu inventory of these locations are not exceeding the forest reference inventory Ref_{for} and would therefore be interpreted as weak soil erosion applying the mass balance model. This is unexpected and can point at a variety of different processes at play not investigated by this study. For example, the measured $^{239+240}$Pu activity at the foot-slope positions may underestimate the $^{239+240}$Pu inventory due to the limited sampling

315   depths of 100 cm. However, an indication for this process would be an increasing $^{239+240}$Pu activity in subsoil, which is not reflected in the data (Fig. 2). Another potential explanation is that $^{239+240}$Pu inventories are reduced due to plant uptake and subsequent plant harvest. However, a substantial plant uptake by crops, like observed for the fallout radionuclide ^{137}Cs (White and Broadley, 2000; Zhu and Smolders, 2000), is unlikely as no elevated $^{239+240}$Pu activity in harvested crops was reported in

other studies (Akleyev et al., 2000). Another potential pathway of soil and $^{239+240}$Pu leaving the cropland plateau sites is harvest
320 erosion associated to commonly cultivated root crops (i.e. cassava, sweet potato, groundnuts). In temperate regions, harvest
erosion rates up to 12 Mg ha^{-1} yr^{-1} have been reported for different crop types (potato: 2.5 - 6 Mg ha^{-1} yr^{-1}; Auerswald and
Schmidt, 1986; Belotserkovsky and Larinovo, 1988; Ruysschaert et al., 2007) (sugarbeet: 5 - 8 Mg ha^{-1} yr^{-1}; Auerswald et al.,
2006) (chicory: 8.1 - 11.8 Mg ha^{-1} yr^{-1}; Poesen et al., 2001). With cassava and sweet potato being the main food crops within
the NiCo region (cassava has a higher proportion on the less fertile soils in the DR Congo, while more sweet potato is cultivated
325 in Uganda), this is a likely source of reduction of $^{239+240}$Pu inventories. To illustrate the potential effect of harvest erosion, a
simple example shows that 5.5 Mg ha^{-1} yr^{-1} of sediment delivery would roughly cause a 20% reduction of the baseline reference
over 55 years (assuming a 20 cm plough depth and 1.35 Mg m^{-2} bulk density). Harvest erosion can be assumed as a process
that has a limited spatial distribution as long as the land use and crop yields are not causing pronounced spatial patterns.
Therefore, in systems where harvest erosion is a relevant driver of $^{239+240}$Pu export, Ref$_{plt}$ would be the valid reference for soil
330 redistribution estimations. However, an accurate estimation on the contribution of $^{239+240}$Pu loss due to harvest erosion since
the 1960s is impossible as limited information is available on soil harvesting loss of cassava and potato by hand cultivation.
Therefore, both Ref$_{for}$ and Ref$_{plt}$ are taken into account within this study to cover the range from a fully preserved to a depleted
$^{239+240}$Pu reference inventory in the study sites.

Soil redistribution in cropland of the NiCo region

335 Both cropland sites show indications of soil redistribution. Particularly the cropland study site in DR Congo shows evidence
for (i) soil loss due to a high number of slope samples falling below the detection limit (50%) and (ii) sedimentation as
evidenced by a clear $^{239+240}$Pu fingerprint in the subsoil of the foot-slope samples. Compared to the Ugandan cropland, the DR
Congo cropland shows a much stronger difference between $^{239+240}$Pu inventories of slope positions and Ref$_{for}$ (Fig. 3). We
340 relate this discrepancy to the varying length since DR Congo and Uganda cropland has been converted from tropical forest.
Forest to cropland conversion at the Ugandan study site took place during the 1970's. Hence, the area was under arable use
for about 40 years compared to 55 years (since the test ban treaty) at the DR Congo study site. Therefore, the Ugandan cropland
was exposed to soil erosion for a roughly 27% shorter time compared to DR Congo cropland. However, the relative $^{239+240}$Pu
inventory reduction at slope sites in Uganda is about 29% compared to Ref$_{for}$, while in DR Congo the relative reduction is
345 83%. The much stronger relative $^{239+240}$Pu reduction in DR Congo cannot be just explained by the shorter cropland use of the
Ugandan cropland site. In direct comparison between the two sites, no major difference regarding slope steepness (12°-13° in
both study sites) and rainfall erosivity (Fenta et al., 2017) were observed. However, the crop rotation between the Ugandan
and DR Congo study site differ substantially, with Uganda being dominated by sweet potato and maize, while DR Congo
cropland is dominated by cassava that may cause different soil erosion conditions.
350 The determined mean soil redistribution rates at cropland slopes found in this study (negative values indicate net erosion and
positive values net sedimentation; DR Congo: -51.4 Mg ha^{-1} yr^{-1} Ref$_{for}$, -1.4 Mg ha^{-1} yr^{-1} Ref$_{plt}$; Uganda: -13.4 Mg ha^{-1} yr^{-1}
Ref$_{for}$, 20.2 Mg ha^{-1} yr^{-1} Ref$_{plt}$) show contrasting results with respect to the assumed reference (Fig. 5). In comparison to values

observed globally (Boardman and Poesen, 2006; Borrelli et al., 2017) the high erosion Ref$_{for}$ simulations are in good agreement with plot monitoring results within the region (mean soil loss of 68.2 Mg ha^{-1} yr^{-1}; Lewis and Nyamulinda, 1996). The range

355   of observed values at slopes spans from net sedimentation to heavy soil loss in direct proximity to each other. This high variation on short spatial distances might be an effect of smallholder farming structures, which mitigate soil loss rates in the NiCo region due to decreasing hydrologic connectivity (Nunes et al., 2018; Baartman et al., 2020) along slopes due to a high degree of "patchiness" and a large number of field boundaries (mean field size 450 m²; Fig. 5). Any conversion of this smallholder farming structure into large scale farming structures, as known from regions with mechanised agriculture, will

360   have devastating effects on soil degradation rates in the region.

5. Conclusions

This study demonstrates the usability of fallout radionuclides ^{239}Pu and ^{240}Pu as a tool to assess soil degradation processes in Tropical Africa. Interpreting $^{239+240}$Pu activity and inventories in soils and organic layers, we assessed soil redistribution rates along three pristine forests catena and in two cropland catchments in the White Nile-Congo rift region. $^{239+240}$Pu inventories in

365   forest did not follow a topography related distribution, indicative for little to no soil erosion. In contrast, cropland sites show signs for substantial soil erosion and sedimentation that exceeds 40 cm over a period of 55 years. However, the selection of an appropriate reference is critical due to a potential $^{239+240}$Pu inventory reduction by harvest erosion in root crop dominated cropland systems. Very high intra-slope variability of the $^{239+240}$Pu inventories in cropland was found (coefficient of variation up to 67%) with sites of pronounced sedimentation in close distance to highly eroded sites, potentially a result of soil cover

370   dynamics due to smallholder farming structures with small fields and individual management. Keeping smallholder farming structures active is essential to mitigate soil degradation in the region, also under current agricultural intensification efforts. Particularly in regions with limited infrastructure and challenging monitoring conditions, $^{239+240}$Pu based soil redistribution analysis can shed light on the pace of soil degradation, which remains a major challenge for future food security in Tropical Africa.

Data availability

375

The data will be made available within the framework of the TropSOC database publication: Doetterl, S., Asifiwe, R.K., Bamba, F., Bukombe, B., Cooper, M., Hoyt, A., Kidinda, K.L., Maier, A., Mainka, M., Mayrock, J., Muhindo, D., Mukotanyi, S.M., Nabahungu, L., Reichenbach, M., Stegmann, A., Summerauer, L., Unseld, R., Wilken, F., Fiener, P.: Organic matter cycling along geochemical, geomorphic and disturbance gradients in vegetation and soils of African tropical forests and

380   cropland - Project TropSOC DATABASE_v1.0, SOIL DISCUSSIONS (in preparation).

Author contribution

This paper represents a result of collegial teamwork. FW, SD, PF and KvO developed the study design. $^{239+240}$Pu activity analysis was carried out by MK. DM carried out the field campaign. Data processing and illustration was carried out by FW. FW, SD, PF, KvO and KM contributed to data analysis and interpretation. FW drafted the manuscript, while all authors reviewed and approved the final version.

Competing interest

The authors declare that they have no conflict of interest.

Acknowledgements

We gratefully acknowledge the outstanding commitment for project TropSOC and fieldwork support of Landry Cizugu, Benjamin Bukombe, Laurent Kidinda, Mario Reichenbach and for labwork Anna Stegmann, Julia Mayrock, Moritz Mainka and Robin Unseld.

References

Akleyev, A. V., Kostyuchenko, V. A., Peremyslova, L. M., Baturin, V. A., and Popova, I. Y.: Radioecological impacts of the Techa River contamination, Health Phys., 79, 36-47, 10.1097/00004032-200007000-00008, 2000.

Alewell, C., Pitois, A., Meusburger, K., Ketterer, M., and Mabit, L.: Pu239+240 from "contaminant" to soil erosion tracer: Where do we stand?, Earth-Sci. Rev., 172, 107-123, 10.1016/j.earscirev.2017.07.009, 2017.

Amundson, R., Berhe, A. A., Hopmans, J. W., Olson, C., Sztein, A. E., and Sparks, D. L.: Soil and human security in the 21st century, Science, 348, 12610711-12610716, 2015.

Angima, S. D., Stott, D. E., O'Neill, M. K., Ong, C. K., and Weesies, G. A.: Soil erosion prediction using RUSLE for central Kenyan highland conditions, Agric., Ecosyst. Environ., 97, 295-308, https://doi.org/10.1016/S0167-8809(03)00011-2, 2003.

Auerswald, K., and Schmidt, F.: Atlas der Erosionsgefährdung in Bayern, GLA-Fachberichte, 1, 1986.

Auerswald, K., Gerl, G., and Kainz, M.: Influence of cropping system on harvest erosion under potato, Soil Till. Res., 89, 22-34, 2006.

Baartman, J. E. M., Nunes, J. P., Masselink, R., Darboux, F., Bielders, C., Degré, A., Cantreul, V., Cerdan, O., Grangeon, T., Fiener, P., Wilken, F., Schindewolf, M., and Wainwright, J.: What do models tell us about water and sediment connectivity?, Geomorphology, 367, 1-17, https://doi.org/10.1016/j.geomorph.2020.107300, 2020.

Belotserkovsky, Y., and Larinovo, A.: Removal of soil by harvest of potatoes and root crops (in Russian), Vestnik Moskovskogo Universiteta Seriia 5: Geografia, 4, 49-54, 1988.

Boardman, J., and Poesen, J.: Soil Erosion in Europe: Major Processes, Causes and Consequences, in: Soil Erosion in Europe, John Wiley & Sons, Ltd, 477-487, 2006.

Borrelli, P., Robinson, D. A., Fleischer, L. R., Lugato, E., Ballabio, C., Alewell, C., Meusburger, K., Modugno, S., Schütt, B., Ferro, V., Bagarello, V., Oost, K. V., Montanarella, L., and Panagos, P.: An assessment of the global impact of 21st century land use change on soil erosion, Nature Communications, 8, 1-13, 10.1038/s41467-017-02142-7, 2017.

Borrelli, P., Robinson, D. A., Panagos, P., Lugato, E., Yang, J. E., Alewell, C., Wuepper, D., Montanarella, L., and Ballabio, C.: Land use and climate change impacts on global soil erosion by water (2015-2070), Proceedings of the National Academy of Sciences, 117, 21994-22001, 10.1073/pnas.2001403117, 2020.

Calitri, F., Sommer, M., Norton, K., Temme, A., Brandova, D., Portes, R., Christl, M., Ketterer, M. E., and Egli, M.: Tracing the temporal evolution of soil redistribution rates in an agricultural landscape using Pu239+240 and Be-10, Earth Surf. Process. Landf., 44, 1783-1798, 10.1002/esp.4612, 2019.

Chamberlin, J., Jayne, T. S., and Headey, D.: Scarcity amidst abundance? Reassessing the potential for cropland expansion in Africa, Food Policy, 48, 51-65, 10.1016/j.foodpol.2014.05.002, 2014.

Chartin, C., Evrard, O., Salvador-Blanes, S., Hinschberger, F., Van Oost, K., Lefevre, I., Daroussin, J., and Macaire, J. J.: Quantifying and modelling the impact of land consolidation and field borders on soil redistribution in agricultural landscapes (1954-2009), Catena, 110, 184-195, 10.1016/j.catena.2013.06.006, 2013.

Doetterl, S., Baert, G., Bauters, M., Boeckx, P., Cadisch, G., Cizungu, L., Hoyt, A., Kabaseke, C., Kalbitz, K., Mujinya, B., Rewald, B., Six, J., Vanlauwe, B., van Oost, K., Verheyen, K., Vogel, C., Wilken, F., and Fiener, P.: Organic matter cycling along geochemical, geomorphic and disturbance gradients in vegetation and soils of African tropical forests and cropland – Project TropSOC, SOIL Discuss., 2021.

Drake, T. W., Van Oost, K., Barthel, M., Bauters, M., Hoyt, A. M., Podgorski, D. C., Six, J., Boeckx, P., Trumbore, S. E., Ntaboba, L. C., and Spencer, R. G. M.: Mobilization of aged and biolabile soil carbon by tropical deforestation, Nat. Geosci., 12, 541-547, 10.1038/s41561-019-0384-9, 2019.

Evans, D. L., Quinton, J. N., Davies, J. A. C., Zhao, J., and Govers, G.: Soil lifespans and how they can be extended by land use and management change, Environmental Research Letters, 15, 1-10, 10.1088/1748-9326/aba2fd, 2020.

Evrard, O., Chaboche, P.-A., Ramon, R., Foucher, A., and Laceby, J. P.: A global review of sediment source fingerprinting research incorporating fallout radiocesium (137Cs), Geomorphology, 362, 1-22, https://doi.org/10.1016/j.geomorph.2020.107103, 2020.

FAO, and ITPS: Status of the World's Soil Resources – Main Report, FAO, Rome, Italy, 2015.

440   Fenta, A. A., Yasuda, H., Shimizu, K., Haregeweyn, N., Kawai, T., Sultan, D., Ebabu, K., and Belay, A. S.: Spatial distribution and temporal trends of rainfall and erosivity in the Eastern Africa region, Hydrol. Processes, 31, 4555-4567, 10.1002/hyp.11378, 2017.

Fick, S. E., and Hijmans, R. J.: WorldClim 2: new 1-km spatial resolution climate surfaces for global land areas, Int. J. Climatol., 37, 4302-4315, https://doi.org/10.1002/joc.5086, 2017.

445   Fiener, P., Wilken, F., and Auerswald, K.: Filling the gap between plot and landscape scale – eight years of soil erosion monitoring in 14 adjacent watersheds under soil conservation at Scheyern, Southern Germany, Adv. Geosci., 48, 31-48, 10.5194/adgeo-48-31-2019, 2019.

Govers, G., Merckx, R., van Wesemae, B., and Van Oost, K.: Soil conservation in the 21st century: why we need smart agricultural intensification, Soil, 3, 45-59, 10.5194/soil-3-45-2017, 2017.

450   Hardy, E. P., Krey, P. W., and Volchok, H. L.: Global inventory and distribution of fallout plutonium, Nature, 241, 444-445, 10.1038/241444a0, 1973.

Kelley, J. M., Bond, L. A., and Beasley, T. M.: Global distribution of Pu isotopes and Np-237, Science of the Total Environment, 238, 483-500, 10.1016/s0048-9697(99)00160-6, 1999.

Ketterer, M. E., Hafer, K. M., Link, C. L., Kolwaite, D., Wilson, J., and Mietelski, J. W.: Resolving global versus local/regional
455   Pu sources in the environment using sector ICP-MS, J. Anal. At. Spectrom., 19, 241-245, 10.1039/b302903d, 2004.

Kottek, M., Grieser, J., Beck, C., Rudolf, B., and Rubel, F.: World map of the Koppen-Geiger climate classification updated, Meteorol. Z., 15, 259-263, 10.1127/0941-2948/2006/0130, 2006.

Lal, R., Tims, S. G., Fifield, L. K., Wasson, R. J., and Howe, D.: Applicability of Pu-239 as a tracer for soil erosion in the wet-dry tropics of northern Australia, Nuclear Instruments & Methods in Physics Research Section B-Beam Interactions with
460   Materials and Atoms, 294, 577-583, 10.1016/j.nimb.2012.07.041, 2013.

Lewis, L. A., and Nyamulinda, V.: The critical role of human activities in land degradation in Rwanda, Land Degrad. Dev., 7, 47-55, 1996.

Meusburger, K., Mabit, L., Ketterer, M., Park, J. H., Sandor, T., Porto, P., and Alewell, C.: A multi-radionuclide approach to evaluate the suitability of Pu239+240 as soil erosion tracer, Science of the Total Environment, 566, 1489-1499,
465   10.1016/j.scitotenv.2016.06.035, 2016.

Montanarella, L., Pennock, D. J., McKenzie, N., Badraoui, M., Chude, V., Baptista, I., Mamo, T., Yemefack, M., Aulakh, M. S., Yagi, K., Hong, S. Y., Vijarnsorn, P., Zhang, G. L., Arrouays, D., Black, H., Krasilnikov, P., Sobocka, J., Alegre, J., Henriquez, C. R., Mendonca-Santos, M. D., Taboada, M., Espinosa-Victoria, D., AlShankiti, A., AlaviPanah, S. K., Elsheikh, E. A. E., Hempel, J., Arbestain, M. C., Nachtergaele, F., and Vargas, R.: World's soils are under threat, Soil, 2,
470   79-82, 10.5194/soil-2-79-2016, 2016.

Nunes, J. P., Wainwright, J., Bielders, C. L., Darboux, F., Fiener, P., Finger, D., and Turnbull, L.: Better models are more effectively connected models, Earth Surf. Process. Landf., 43, 1355-1360, https://doi.org/10.1002/esp.4323, 2018.

Nyesheja, E. M., Chen, X., El-Tantawi, A. M., Karamage, F., Mupenzi, C., and Nsengiyumva, J. B.: Soil erosion assessment using RUSLE model in the Congo Nile Ridge region of Rwanda, Physical Geography, 40, 339-360,
475   10.1080/02723646.2018.1541706, 2019.

Nyssen, J., Poesen, J., Moeyersons, J., Deckers, J., Haile, M., and Lang, A.: Human impact on the environment in the Ethiopian and Eritrean highlands - a state of the art, Earth-Sci. Rev., 64, 273-320, 10.1016/s0012-8252(03)00078-3, 2004.

Poesen, J. W. A., Verstraeten, G., Soenens, R., and Seynaeve, L.: Soil losses due to harvesting of chicory roots and sugar beet: an underrated geomorphic process?, Catena, 43, 35-47, 2001.

480   Porto, P., and Walling, D. E.: Using plot experiments to test the validity of mass balance models employed to estimate soil redistribution rates from 137Cs and 210Pb-ex measurements, Appl. Radiat. Isot., 70, 2451-2459, 10.1016/j.apradiso.2012.06.012, 2012.

R: A Language and Environment for Statistical Computing: https://www.R-project.org/, access: 27.10.2020, 2019.

Reichenbach, M., Fiener, P., Garland, G., Six, S., and Doetterl, S.: The role of geochemistry in organic carbon stabilization in
485   tropical rainforest soils, SOIL Discuss., 2021.

Ruysschaert, G., Poesen, J., Auerswald, K., Verstraeten, G., and Govers, G.: Soil losses due to potato harvesting at the regional scale in Belgium, Soil Use Manag., 23, 156-161, 2007.

Ryan, J. N., Illangasekare, T. H., Litaor, M. I., and Shannon, R.: Particle and plutonium mobilization in macroporous soils during rainfall simulations, Environmental Science & Policy, 32, 476-482, 1998.

490   van Ittersum, M. K., van Bussel, L. G. J., Wolf, J., Grassini, P., van Wart, J., Guilpart, N., Claessens, L., de Groot, H., Wiebe,
         K., Mason-D'Croz, D., Yang, H., Boogaard, H., van Oort, P. A. J., van Loon, M. P., Saito, K., Adimo, O., Adjei-Nsiah, S.,
         Agali, A., Bala, A., Chikowo, R., Kaizzi, K., Kouressy, M., Makoi, J. H. J. R., Ouattara, K., Tesfaye, K., and Cassman, K.
         G.: Can sub-Saharan Africa feed itself?, Proceedings of the National Academy of Sciences, 113, 14964-14969,
         10.1073/pnas.1610359113, 2016.

495   Wallbrink, P. J., and Murray, A. S.: Use of radionuclides as indicators of erosion processes, Hydrol. Processes, 7, 297-304,
         10.1002/hyp.3360070307, 1993.

         White, P. J., and Broadley, M. R.: Mechanisms of caesium uptake by plants, New Phytol., 147, 241-256, 10.1046/j.1469-
         8137.2000.00704.x, 2000.

         Wilcke, W., Yasin, S., Abramowski, U., Valarezo, C., and Zech, W.: Nutrient storage and turnover in organic layers under
500   tropical montane rain forest in Ecuador, Eur. J. Soil Sci., 53, 15-27, 10.1046/j.1365-2389.2002.00411.x, 2002.

         World Population Review: https://worldpopulationreview.com, access: 13.12.2020, 2020.

         WRB: World reference base for soil resources 2006, FAO, Rome, 1-145, 2006.

         Xiong, M. Q., Sun, R. H., and Chen, L. D.: A global comparison of soil erosion associated with land use and climate type,
         Geoderma, 343, 31-39, 10.1016/j.geoderma.2019.02.013, 2019.

505   Zhang, H., Aldana-Jague, E., Clapuyt, F., Wilken, F., Vanacker, V., and Van Oost, K.: Evaluating the potential of post-
         processing kinematic (PPK) georeferencing for UAV-based structure-from-motion (SfM) photogrammetry and surface
         change detection, Earth Surf. Dynam., 7, 807-827, 10.5194/esurf-7-807-2019, 2019.

         Zhu, Y. G., and Smolders, E.: Plant uptake of radiocaesium: a review of mechanisms, regulation and application, J. Exp. Bot.,
         51, 1635-1645, 10.1093/jexbot/51.351.1635, 2000.

510

Tables

Table 1: Numbers of samples taken at three forest and two cropland study sites (DR Congo, Uganda, Rwanda). Please note that data on cropland does not include study sites in Rwanda (L = L horizon; O = O horizon; M = mineral layer 1: 0-60 cm and 2: 60-120 in forest and 60-100 cm in cropland). While the O horizon depth is measured individually for each sample, the L horizon depth is assumed to be 1 cm as it was not possible to be accurately measured.

	Forest		
	Plateau	Slope	Foot-slope
L, O, M1	10	6	6
M2	0	0	6
	Cropland		
	Plateau*	Slope	Foot-slope
M1	12	27	12
M2	0	0	12

*Three depth increments 0 - 20 cm, 20 - 40 cm, 40 - 60 cm

Figures
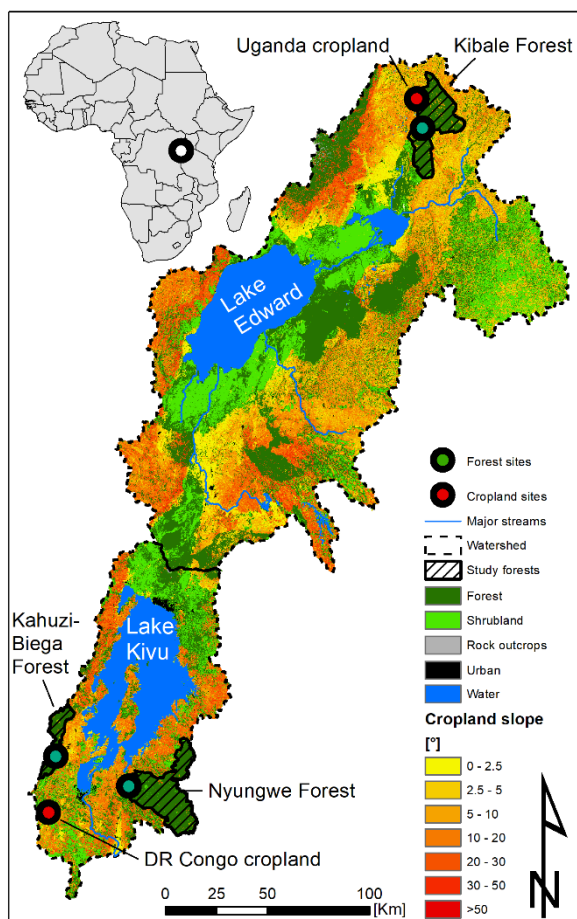
520   Figure 1: Study area, locations of forest and cropland sites, topography and land use in the White Nile-Congo rift region.
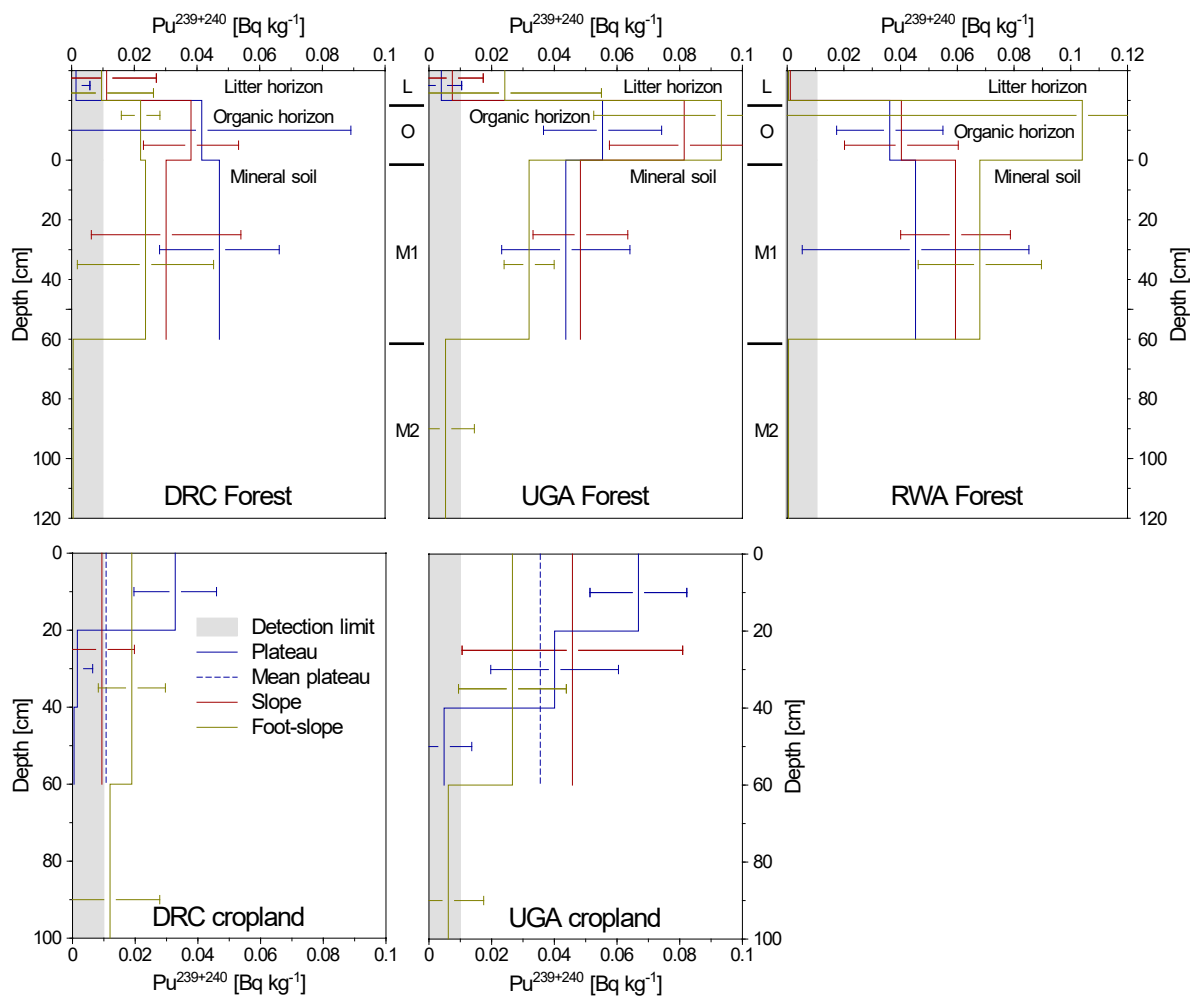
Figure 2: Catenae related depth profiles of $^{239+240}$Pu activity and standard deviations (whisker) within three pristine

forests (DRC: DR Congo, UGA: Uganda, RWA: Rwanda) and two cropland study sites. Please note that the L and

525 O horizons are for illustrational purposes shown thicker than they naturally appear.
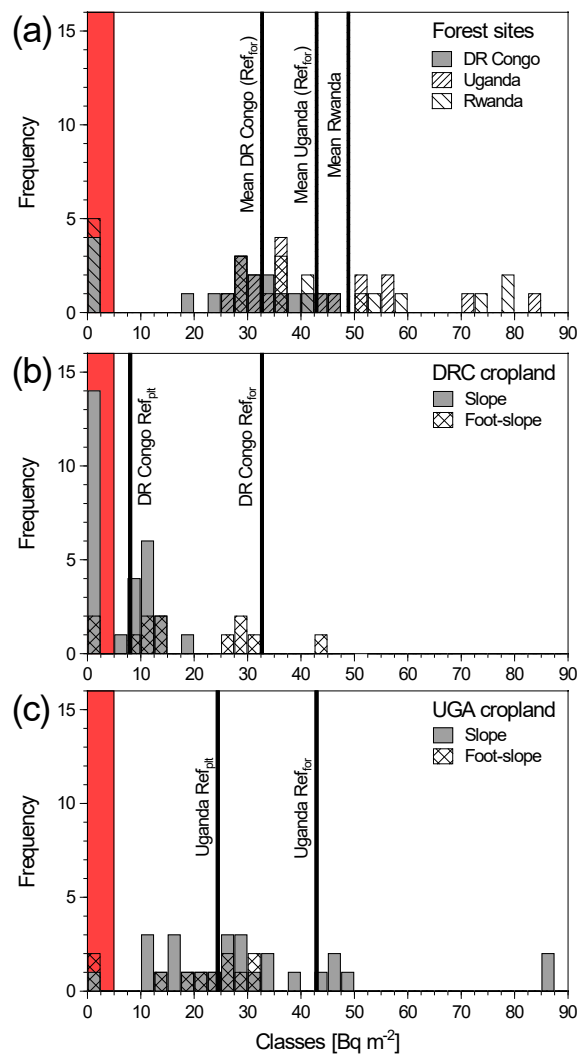
Figure 3: Distribution of $^{239+240}$Pu inventories in three forests and two cropland study sites. In (a) the $^{239+240}$Pu histogram for three forest sites is given, while (b) and (c) represent the cropland distribution at the slope and foot-slope topographic positions. The vertical lines represent the mean values serving as forest reference (Ref$_{for}$) and cropland plateau reference (Ref$_{plt}$). Red section at the left of the graphs illustrate the detection limit.
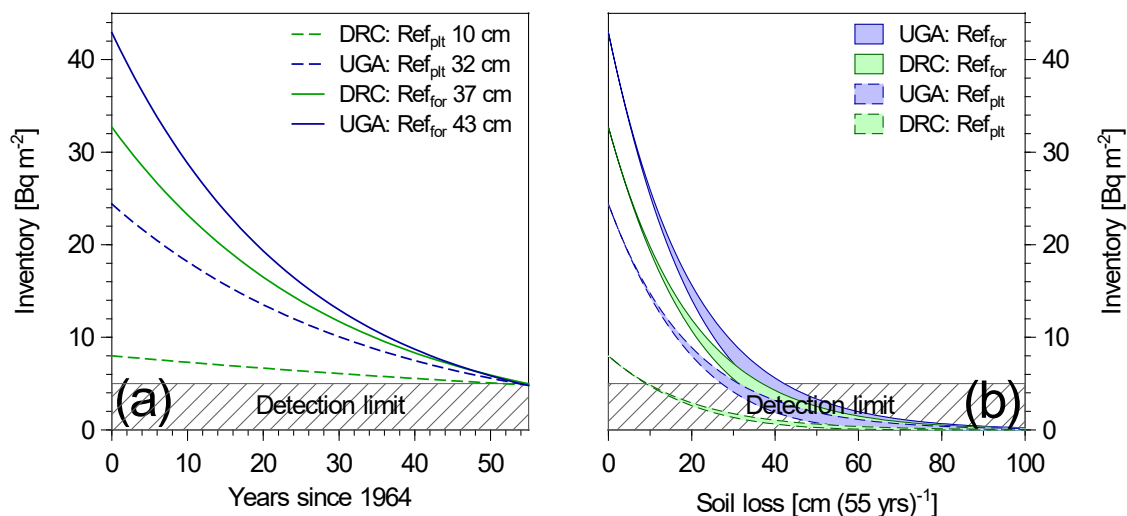
Figure 4: DR Congo (DRC) and Uganda (UGA) cropland soil erosion results of the mass balance model. A scenario
535   assessment was carried out to understand $^{239+240}$Pu inventory reduction until detection limit is reached after the
simulation period: (a) soil erosion magnitude and corresponding (b) soil erosion frequency according to the mean
forest (Ref$_{for}$) and mean cropland plateau (Ref$_{plt}$) assumption. (a) Represents the minimum quantity of soil erosion
to pass the detection limit of different reference $^{239+240}$Pu inventories. All displayed curves show the corresponding
scenario runs of minimum soil erosion to cause a $^{239+240}$Pu inventory reduction that falls below the detection limit.
540   (b) Comparison between a continuous 55 years soil erosion rate vs. 5 erosive years that cause the same quantity of
soil erosion. Soil erosion from 1 to 100 cm (55 yrs)$^{-1}$ is simulated. The coloured area describes the difference
between the two scenarios, where the lower line is the 5 year scenario.
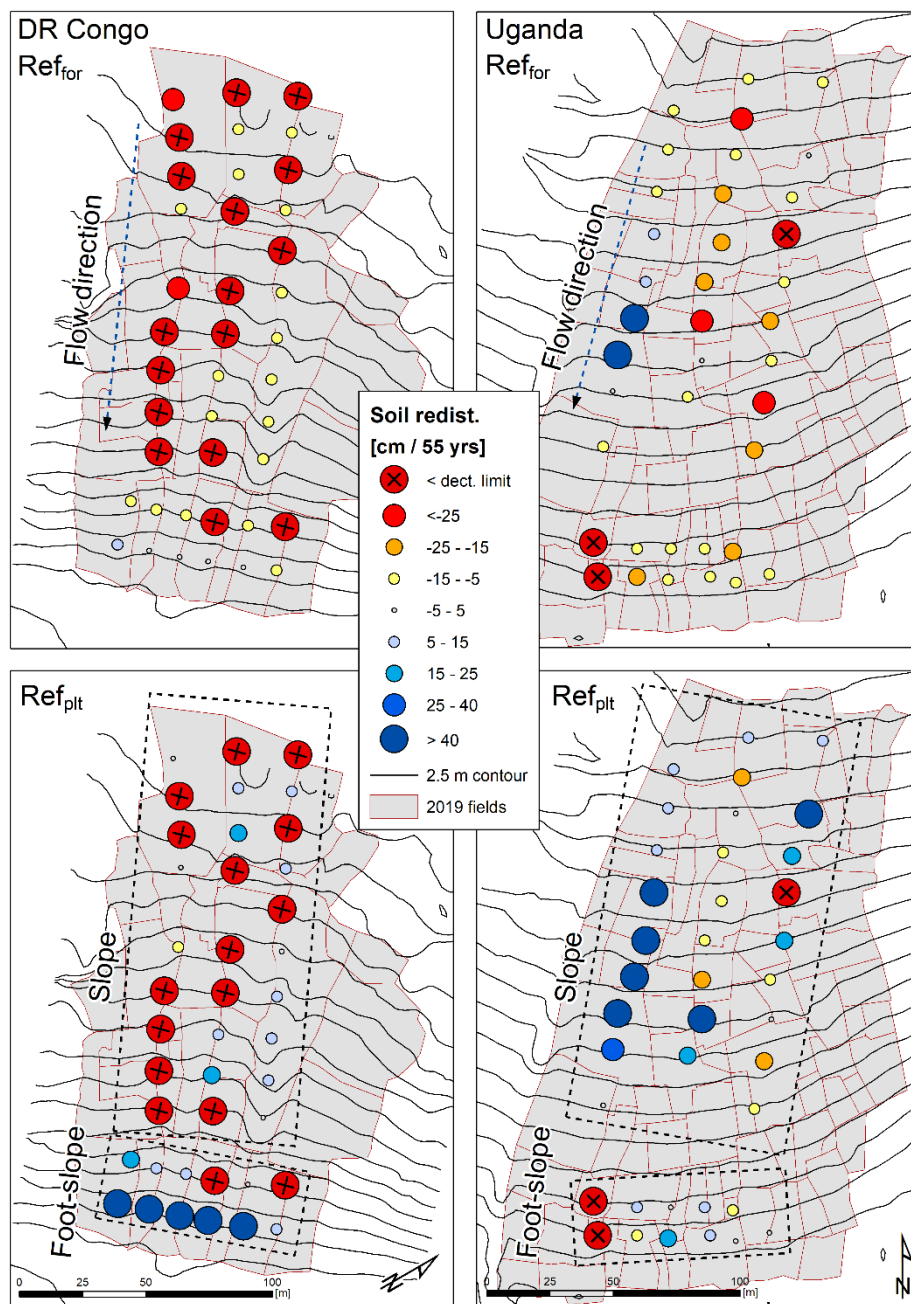
Figure 5: Soil redistribution derived from $^{239+240}$Pu measurements using a mass balance model. Two different reference inventories (upper: Ref_{for} = mean forest reference; lower: Ref_{plt} mean cropland plateau reference) in two cropland areas of the White Nile-Congo rift region (left: DR Congo, right: Uganda) were analysed.